A Linearized Analysis of Diurnal Boundary Layer Convergence over the Topography of the United States

JAN PAEGLE[1]

National Center for Atmospheric Research,[2] Boulder, Colo. 80307

(Manuscript received 9 August 1977, in final form 12 December 1977)

ABSTRACT

A linearized model of forced Boussinesq, hydrostatic, gravity inertia waves is developed in a terrain-following coordinate system. Diurnally periodic motions, forced by diurnally fluctuating buoyancy forces above sloping terrain, are studied through particular solutions that represent bounds to the complete solutions. The present results suggest that gently sloping terrains exert important controls on convective activity through boundary layer convergence generation. The model solutions appear to be most sensitive to details of the diurnally oscillating thermal boundary layer. They are also rather sensitive to synoptic-scale ambient circulations as well as dissipation, but apparently less sensitive to horizontal variations of stratification.

1. Introduction

A comprehensive documentation of thunderstorm activity over the United States by Wallace (1975) displays a remarkable diurnal modulation of summer convection. Since the summer atmosphere over most of the United States is often convectively unstable both day and night, it is reasonable to suppose that the diurnal control of convection is due to lifting of moist low-level air.

The pronounced nocturnal convection over the central United States has attracted particular attention. Wallace (1975), Lettau (1967), Bonner (1966) and others have presented evidence that, here, the diurnally oscillating boundary layer convergence field that is induced by the solar cycle above sloping terrain, is a major control.

Although some simplified models have been constructed to predict nocturnal boundary layer convergence (e.g., Paegle and McLawhorn, 1973), detailed numerical prediction of nocturnal boundary layer convergence fields over realistic terrain has received relatively little attention. Large-scale numerical models currently lack the vertical resolution required to simulate the detailed vertical structure of the lower planetary boundary layer. Mesoscale studies (Pielke and Mahrer, 1975) conclude that eight computation levels are sufficient to resolve the daytime boundary layer, but it is not obvious that this is enough for the nocturnal boundary layer that commonly contains pronounced inversions and sharp jets. Paegle and McLawhorn (1973), Welch *et al.* (1978) and other investigators of the vertical profiles of diurnally varying boundary layers generally retain more computational levels in the vertical.

Detailed numerical prediction of boundary layer convergence is limited due to the computational expense associated with vertical resolution. The few published studies that claim to do this (Pielke, 1974; Paegle and Rasch, 1973; Paegle and McLawhorn, 1973) do so only in localized regions and generally ignore or minimize the influence of larger scale aspects of the flow. Consequently, the modulation of the boundary layer response by ambient conditions is not very well understood. This is the reason for the present study.

The present investigation relaxes certain assumptions inherent in the model used by Paegle and Rasch and by Paegle and McLawhorn, by permitting the model pressure field to be modified by the convergence field. The resulting system contains gravity wave modes, excluded in our prior modeling. For the scales in question, a Boussinesq, hydrostatic, gravity inertia wave model represents a consistent approach (Section 2). Poleward of 30° latitude, the solutions exhibit external wave behavior for diurnally forced motions (Section 3). Thus, unlike most mesoscale gravity waves, this type does not require ducts (e.g., Lindzen and Tung, 1976) in order to exhibit significant energy concentrations around the levels of excitation.

The vertical structure of the solutions varies as

$$Ae^{-z/H} - Be^{-z/D}$$

with D and H magnitudes on the order of a few hundred meters. This height dependence is simulated analytically, thereby avoiding the computational expense of the grid-point models.

[1] On leave from the Department of Meteorology, University of Utah, Salt Lake City, Utah 84112.

[2] The National Center for Atmospheric Research is sponsored by the National Science Foundation.

0027-0644/78/0492-0502$05.50

The goal of the present study is to perform experiments of the sensitivity of the response of the topographically induced boundary layer convergence fields over the United States to ambient conditions, such as dissipation, stratification, absolute rotation and the vertical structure of the forcing. For this purpose it is not necessary to obtain complete solutions. It is argued in Section 3 that certain partial particular solutions represent reasonable bounds to the complete solutions. Such particular solutions are described in Section 4. They indicate sensitivity to dissipation, to boundary layer heating and its vertical extent, as well as to the ambient circulation. Implications for more complete forecasting models are given in Section 5.

2. Model

a. Equations

The analysis is based on the standard anelastic system of equations linearized about a basic state at rest:

$$L(\mathbf{V}^*)+f\mathbf{K}\times\mathbf{V}^*=-\nabla_H P'+\mathbf{F} \tag{1}$$

$$L(w^*)=-\frac{\partial P'}{\partial z}-\rho' g \tag{2}$$

$$\nabla_H\cdot\mathbf{V}^*+\frac{\partial w^*}{\partial z}=0 \tag{3}$$

$$L(P')+\frac{w^*}{\bar\rho}\frac{\partial\bar P}{\partial z}=\frac{\bar P\gamma}{\bar\rho}\left[L(\rho')+\frac{w^*}{\bar\rho}\frac{\partial\bar\rho}{\partial z}\right]+Q\bar\rho(\gamma-1). \tag{4}$$

Symbols are defined as follows:

γ	ratio of specific heat constants $[=c_p/c_v]$
$\mathbf{V}^*$	$\bar\rho\mathbf{V}'$
w^*	$\bar\rho w'$
Q	heating
$\bar\rho$	basic-state density
$\bar p$	basic-state pressure
p'	perturbation pressure
ρ'	perturbation density
$\mathbf{V}'$	perturbation horizontal velocity $[=(u'\mathbf{i}+v'\mathbf{j})]$
w'	perturbation vertical velocity
f	Coriolis parameter
$\mathbf{F}$	forcing term (to be specified)
∇	$\mathbf{i}\frac{\partial}{\partial x}+\mathbf{j}\frac{\partial}{\partial y}$
L	$\left(\frac{\partial}{\partial t}-K\frac{\partial^2}{\partial z^2}\right)$
K	eddy mixing coefficient.

The scale analysis for anelastic motions is given by Ogura and Phillips (1962).

The assumption of a resting basic state will be relaxed in Section 4 to include large-scale circulations in one experiment. However, vertical shears in the ambient flow and related instabilities will be suppressed.

Eqs. (1)–(3) may be combined into a single equation in w^*, i.e.,

$$-\nabla^2[L^2(w^*)]-\left[\frac{\partial}{\partial z}\left(\frac{\partial}{\partial z}+\frac{g}{C^2}\right)\right]L^2(w^*)$$
$$-\nabla^2(N^2w^*)-\left[\frac{\partial}{\partial z}\left(\frac{\partial}{\partial z}+\frac{g}{C^2}\right)\right]f^2w^*$$
$$=\left[\frac{\partial}{\partial z}+\frac{g}{C^2}\right]L(\nabla\cdot\mathbf{F})-\nabla^2\left[Q(\gamma-1)\bar\rho\frac{g}{C^2}\right], \tag{5}$$

where $C^2=\gamma R\bar T$, $N^2=g\,\partial\ln\bar\theta/\partial z$ and $\bar T$, $\bar\theta$ are the basic-state temperature and potential temperature. Gradients of f (β terms) have been neglected here, excluding Rossby wave modes from the present solutions.

If the hydrostatic assumption is made, the first term of (5) vanishes. Furthermore, if the vertical scale of the motion is small with respect to C^2/g (roughly the atmospheric scale height of about 13 km), the Boussinesq approximation is valid, and (5) simplifies to

$$-[L^2+f^2]\frac{\partial^2 w'}{\partial z^2}-\nabla^2(N^2w')$$
$$=-\frac{1}{\bar\rho}\frac{\partial}{\partial z}L(\nabla\cdot\mathbf{F})-\nabla^2\left[Q(\gamma-1)\frac{g}{C^2}\right]. \tag{6}$$

b. Terrain following coordinates

A similar analysis may be performed in the terrain-following coordinate system used by Holton (1967). $\mathbf{V}'$ and w' now represent velocity components parallel and perpendicular to the terrain, respectively, x and y are nearly eastward and northward distances measured on surfaces parallel to the terrain, and z is distance above the surface measured along the local normal to the surface.

These terrain-following coordinates are useful for the present study of shallow flow above variable topography. The main advantage of the present orthogonal coordinates over other terrain-following non-orthogonal systems (e.g., sigma coordinates) is the fact that horizontal derivatives can be numerically well determined, even near sloping terrain. A completely consistent derivation of the following equations is beyond the scope of the present study, but our analysis (to be reported later) indicates that all of the manipulations following in (7)–(15) are consistent order of magnitude approximations if the magnitude of the terrain slope does not exceed 1/100, and the magnitude of the terrain curvature does not exceed 10^{-4} m^{-1}. The terrain used is displayed in Figs. 2 and 3. The

terrain slopes are everywhere less than 10^{-2}, and curvatures are less than 10^{-4} m^{-1}.

If, in addition to these assumptions, the standard anelastic, hydrostatic, and small-Rossby-number assumptions (e.g., Haltiner, 1971, Chap. 3) are satisfied, the equations can be shown to reduce to

$$L(u^*)-fv^*\cos\delta+fw^*\sin\beta = -\frac{\partial(\bar{p}+p')}{\partial x}-g(\bar{\rho}+\rho')\sin\alpha, \quad (7)$$

$$L(v^*)+fu^*\cos\delta-fw^*\sin\alpha = -\frac{\partial(\bar{p}+p')}{\partial x}-g(\bar{\rho}+\rho')\sin\beta, \quad (8)$$

$$L(w^*)+fv^*\sin\alpha-fu^*\sin\beta = -\frac{\partial(\bar{p}+p')}{\partial z}-g\cos\gamma, \quad (9)$$

$$w'\frac{\partial\bar{\rho}}{\partial z}+u'\frac{\partial\bar{\rho}}{\partial x}+v'\frac{\partial\bar{\rho}}{\partial y} = -\bar{\rho}\left(\frac{\partial w'}{\partial z}+\frac{\partial u'}{\partial x}+\frac{\partial v'}{\partial y}\right), \quad (10)$$

$$L(p') = -C^2\left[w^*\frac{\partial\ln\bar{\theta}}{\partial z}+u^*\frac{\partial\ln\bar{\theta}}{\partial x}+v^*\frac{\partial\ln\bar{\theta}}{\partial y}\right] +L(\rho')C^2+Q\bar{\rho}(\gamma-1). \quad (11)$$

Here α, β, δ are the angles measured from the previous horizontal (x,y,z) coordinate axes to the new terrain following (x,y,z) coordinates, respectively. Nonlinear terms, whose relative magnitudes scale with the Rossby number, are neglected.

A further scale analysis then indicates that for shallow Boussinesq and hydrostatic perturbations in a resting basic state, Eqs. (7)–(10) are well approximated by

$$L(u')-fv' = -\frac{1}{\bar{\rho}}\frac{\partial P'}{\partial x}+g\frac{T'}{\bar{T}}\sin\alpha, \quad (12)$$

$$L(v')+fu' = -\frac{1}{\bar{\rho}}\frac{\partial P'}{\partial y}+g\frac{T'}{\bar{T}}\sin\beta, \quad (13)$$

$$\frac{\partial P'}{\partial z} = -\rho' g, \quad (14)$$

$$\frac{\partial w'}{\partial z}+\left(\frac{\partial u'}{\partial x}+\frac{\partial v'}{\partial y}\right)=0, \quad (15)$$

where $\bar{T}$ is the basic state temperature.

If it also is assumed that the basic state develops isentropic surfaces that are locally parallel to the terrain, Eq. (11) becomes

$$L(\rho') = \bar{\rho}w'\frac{\partial\ln\bar{\theta}}{\partial z}-\frac{Q\bar{\rho}(\gamma-1)}{C^2}. \quad (16)$$

The assumption that isentropes align with the surface is most restrictive near steep terrain, and less important near gentle slopes.

c. *Buoyancy effect*

The idealized motion is generated through the T' terms of (12) and (13). These terms represent the component of gravitational acceleration parallel to the terrain slope, and produce slope circulations whenever the T' term (buoyancy effect) is nonzero. In the present case, the buoyancy forces are driven by the solar cycle above sloping terrain. Holton (1967) studied a horizontally uniform low-level jet with a similar approach.

It is useful to split (16) into the following two equations:

$$L(\rho_1') = \bar{\rho}w'\partial\ln\bar{\theta}/\partial z, \quad (17)$$

$$L(\rho_2') = Q\bar{\rho}(\gamma-1)/C^2, \quad (18)$$

where $\rho' = \rho_1' + \rho_2'$.

If ρ_2' is horizontally uniform, its contribution to P' is horizontally uniform [Eq. (14)], and ρ_2' cannot affect gradients of the p' field. This is the case if $Q\bar{\rho}/C^2$ is horizontally uniform in the present coordinate system, implying that radiative processes are independent of terrain height. With this assumption we may replace ρ' with ρ_1' in (14).

Furthermore, since

$$\rho'/\bar{\rho} \approx p'/\bar{p}-T'/\bar{T},$$

and since

$$p'/\bar{p} \ll T'/\bar{T},$$

for a hydrostatic flow possessing a vertical scale much less than C^2/g, we can write

$$\rho' \approx -\bar{\rho}T'/\bar{T}$$

for the present Boussinesq (shallow) flow.

The assertion that

$$L(T') = -Q\bar{T}(\gamma-1)/C^2 \quad (19)$$

is therefore reasonable if the temperature changes associated with the gravity wave are much smaller than those due directly to the solar cycle.

The mathematically simplest, relevant version of (19) proceeds with an exponentially height damping, diurnally periodic heating function (e.g., Holton, 1967). This leads to diurnally periodic temperature variations that damp exponentially in height (as $e^{-z/300\text{ m}}$), and have temperature phase lags of about 2 h between the surface and 500 m, (Paegle, 1969). The small vertical phase lag will be ignored here, and the specification for T' will assume the form

$$T' = \Upsilon e^{i\omega t}e^{-z/H}, \quad \omega = 2\pi/24\text{ h}, \quad H = 300\text{ m}, \quad (20)$$

where Υ is the magnitude of the surface diurnal temperature wave. Solutions retaining the vertical phase lag in T' (not shown) are similar to those that do not.

Eqs. (12)–(16) are mathematically equivalent to the Boussinesq, hydrostatic version of (1)–(4), with $(\bar{\rho}gT'/\bar{T})[\sin(\alpha)\mathbf{i}+\sin(\beta)\mathbf{j}]$ assuming the role of $\mathbf{F}$. Therefore, to a good approximation, (6) also governs the component of motion perpendicular to the terrain, and the governing equation is (omitting primes for brevity)

$$-[L^2+f^2]\frac{\partial^2 w}{\partial z^2}-\nabla^2(N^2w)=\frac{g}{\bar{T}}\frac{\partial}{\partial z}\{\nabla^2(Z_T)L(T')\}. \quad (21)$$

Heating rates have been assumed to be independent of (x,y) on the sloping terrain. Here Z_T represents terrain height and

$$\sin\alpha\approx\frac{\partial Z_T}{\partial x}, \quad \sin\beta\approx\frac{\partial Z_T}{\partial y}$$

have been used.

3. Nature of solutions

The solution of (17) represents a difficult problem for any realistic terrain resolutions, and it may be easier to solve the more general systems (7)–(11) or (12)–(15) numerically. However, that presents the practical computational problems outlined in the Introduction, and it is useful to anticipate the sensitivity of the solutions to various physical effects before undertaking this task.

a. Particular solutions

Particular solutions of (21) provide useful bounds to complete solutions of (21). This conclusion is developed in the present section.

Substitution of the temperature field into (21) gives

$$-[L^2+f^2]\frac{\partial^2 w}{\partial z^2}-\nabla^2(N^2w)$$
$$=g\nabla^2(Z_T)L[\Upsilon e^{-z/H}e^{i\omega t}]/(-\bar{T}H). \quad (22)$$

The solution of (22) reduces to the solution of

$$w=w_P+w_H,$$

where w_P is any solution of

$$-[L^2+f^2]\frac{\partial^2 w_P}{\partial z^2}-\nabla^2(N^2w_P)$$
$$=-(g/\bar{T})\nabla^2(Z_T)L[\Upsilon e^{-z/H}e^{i\omega t}]/H \quad (23)$$

and w_H satisfies

$$-[L^2+f^2]\frac{\partial^2 w_H}{\partial z^2}-\nabla^2(N^2w_H)=0, \quad (24)$$

with boundary conditions

$$\left.\begin{aligned} &w_H(x,y,z=0,t)=-w_P(x,y,z=0,t)\\ &w \text{ bounded as } x\to\pm\infty\\ &\qquad\qquad y\to\pm\infty\\ &\qquad\qquad z\to+\infty \end{aligned}\right\}.$$

One particular solution of (23) has the form

$$w_P=W(x,y,t)e^{-z/H}, \quad (25)$$

where $W(x,y,t)$ satisfies

$$\left[\left(\frac{\partial}{\partial t}+\nu'\right)^2+f^2\right]W/H^2+\nabla^2(N^2W)$$
$$=\frac{g\Upsilon}{\bar{T}}\nabla^2Z_T\frac{i\omega+\nu'}{H}e^{i\omega t}, \quad (26)$$

where $\nu'=K/H^2$.

The fact that (26) is an elliptic equation in time is partly an artifact of the problem decomposition, since each forecast equation from which (26) derives is parabolic if friction is retained. Nevertheless, (26) may not be mathematically solvable with an initial value approach [e.g., the Hadamard counter-example (Garabedian, 1964, p. 108)]. For a well-posed problem it is necessary to respecify (26) as a boundary value problem in three dimensions (x,y,t), with initial data assigned only on W at $t=0$ and again on W as $t\to\infty$. In the frictional care, for spatially periodic, bounded solutions, the latter cannot influence results at finite time, for which we may assume behavior of the form

$$W\propto e^{i\omega t},$$

thereby avoiding the initial value approach.

b. Upper bounds

The partial solutions given by (25) are of practical interest because their associated low-level convergence fields give upper bounds to the low-level convergence fields of entire solutions.

In order to motivate the upper bound character of the particular solutions it is useful to temporarily consider a Cartesian geometry and solutions having sinusoidal behavior in x and y. Expansion of the right-hand side of (23) into a two-dimensional Fourier sum, whose individual contributions are such that

$$\frac{\Upsilon g}{\bar{T}}\frac{(i\omega+\nu')}{H}\nabla^2Z_T=A_{kl}e^{i(kx+ly)}, \quad (27)$$

gives periodic particular solutions composed of sums of expressions of the form

$$w_{Pkl}=A_{kl}e^{i(kx+ly+\omega t)}e^{-z/H}B^{-1}, \quad (28)$$

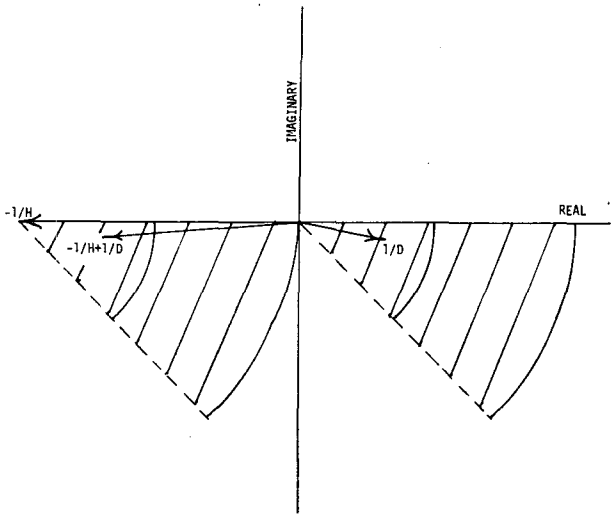

FIG. 1. The relationship of homogeneous, particular and total surface convergence solution coefficients. The arrow points at $1/D$, $-1/H$, $-1/H+1/D$ denote the homogeneous, particular and total solution coefficients, respectively, for the example given in the text. The hatched region on the right denotes the possible range of homogeneous solutions for which $|D|>H$, and the hatched region to the left denotes the corresponding range of the total solutions. The large arcs delimit wavelengths >500 km, small arcs delimit wavelengths >1000 km. The depiction applies to any latitude and $H=300$ m, $\nu=10^{-5}$ s^{-1}, $\omega=2\pi/24h$.

where

$$B=H^{-2}[(i\omega+\nu')^2+f^2]-N^2(k^2+l^2).$$

For each component of w_P in Eq. (28) there must be corresponding components to the homogeneous solution of the form

$$w_{Hkl}=\sum_{j=1}^{3} A_j e^{i(kx+ly+\omega t)}e^{-z/D_j}B^{-1}, \qquad (29)$$

where

$$\sum_{j=1}^{3} A_j=-A_{kl}$$

in order that the condition of zero w is satisfied at the surface. Here,

$$D_j^2=[(i\omega+K/D_j)^2+f^2]/[N^2(k^2+l^2)]. \qquad (30)$$

In order to satisfy the upper boundary condition it is necessary to select the three roots of D_j for which the real parts are positive. Friction (K) ensures that the resulting solutions are vertically trapped regardless of latitude. Of course, vertical trapping occurs poleward of 30° latitude (where $f^2>\omega^2$) even in the frictionless case.

The three roots of (30) possessing negative real parts all have magnitudes larger than H for synoptic space scales and $K\gtrsim 25$ m^2/s^{-1}. For these cases, the low-level convergence ($\partial w/\partial z$) is dominated by the particular solution. Further inspection of these roots and the actual data summarized in Section 3c below suggests that the terrain-induced convergence fields are bounded by the particular solutions even for smaller scales and diffusivities. However, the strength of these bounds cannot be precisely given without introducing lower boundary conditions. This, in turn, requires retention of a surface boundary layer with variable K, significantly complicating the present analysis.

Therefore, an estimate of the strength of the particular solution bound will be given for the case that the operator L is simplified to

$$L(\ )=\left(\frac{\partial}{\partial t}+\nu\right)(\ ).$$

The substitution of a drag formulation for frictional effects is not critical to the argument of Section 3c, although it will be retained subsequently for conciseness.

The complete solution for mode (k,l) is then

$$w_{kl}=A_{kl}e^{i(kx+ly+\omega t)}[e^{-z/H}-e^{-z/D}]B^{-1}, \qquad (31)$$

with D, B satisfying

$$\left.\begin{aligned} D^2&=[(i\omega+\nu)^2+f^2]/[N^2(k^2+l^2)]\\ B&=[(i\omega+\nu)^2+f^2]H^{-2}-N^2(k^2+l^2)\end{aligned}\right\}. \qquad (32)$$

The related divergence is

$$\frac{\partial w_{kl}}{\partial z}=-A_{kl}e^{i(kx+ly+\omega t)}B^{-1}[-H^{-1}e^{-z/H}+D^{-1}e^{-z/D}]. \qquad (33)$$

Poleward of 30°, for modes with $|D|>H$, the magnitude of the total surface divergence is bounded by the magnitude of the particular solution, because the

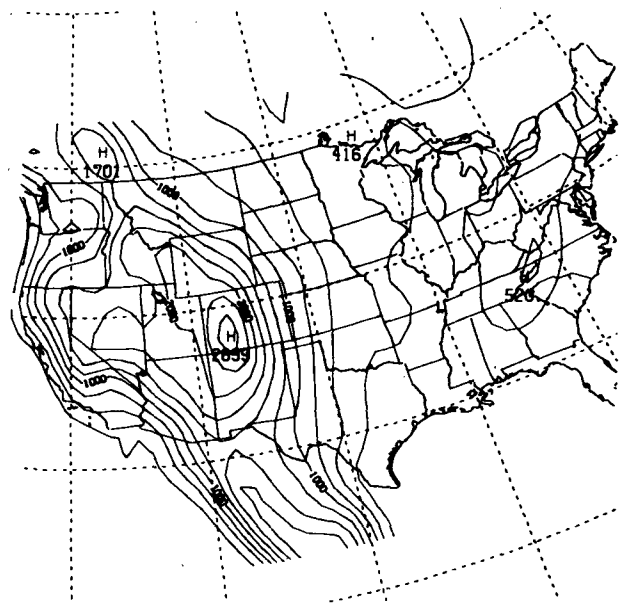

FIG. 2. The terrain height (m).

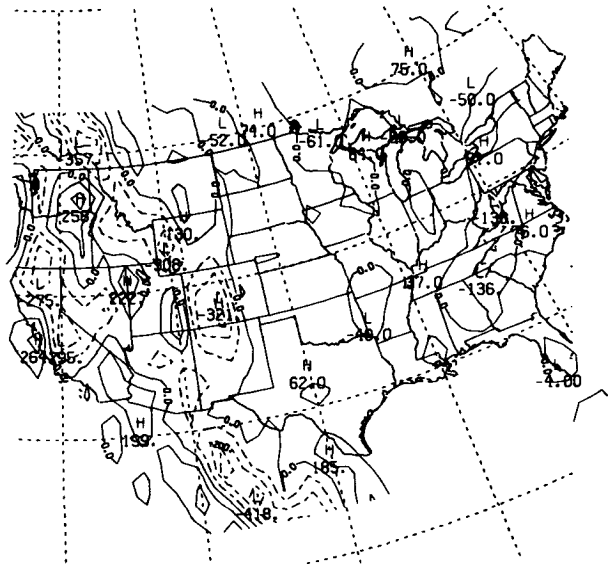

FIG. 3. The terrain Laplacian (10^{-10} m^{-1}).

phase differences of the two contributions must lie between $3\pi/4$ and π. This can be argued from the geometry of Fig. 1, which can also be used to demonstrate that the particular solution lags the total solution by less than 90° for modes with $|D|>H$.

As an example, at 40°, with $k^2+l^2=(2\pi/10^6\text{ m})^2$, $\nu=10^{-5}$ s^{-1}, $\omega=2\pi/24$ h, the value of D is $(978+190i)$ m. In this case

$$-H^{-1}+D^{-1}=-0.0023-0.0002i,$$

showing that the particular solution surface divergence (-0.0033) has about 33% more magnitude, and 5° phase lag with respect to the total solution for this mode (see Fig. 1).

c. *Observational evidence for vertical structure*

It remains to be demonstrated that scales for which $H<|D|$ in fact dominate shorter scales for which $H>|D|$. This can be done by comparing the model predicted force fields with observations.

From (14) we have

$$L(P')=-g\int_z^\infty L(\rho')dz,$$

and from (16a) and (25)

$$(LP')=(\bar{\rho}N^2)\int_z^\infty w'dz$$

$$=A_{kl}e^{i(kx+ly+\omega t)}[He^{-z/H}-De^{-z/D}]\bar{\rho}N^2B^{-1}, \quad (34)$$

for mode (k,l). Thus, the gravity wave associated pressure field is given by sums of

$$P'_{kl}=A_{kl}e^{i(kx+ly+\omega t)}[He^{-z/H}-De^{-z/D}]\bar{\rho}N^2/[B(i\omega+\nu)].$$

Since the driving force [T' terms of (12), (13)] has the same damping rate as the particular solution, the relative phase of the particular solution pressure force with respect to the driving force is independent of height. Therefore, phase changes of the total horizontal force field can occur only due to the homogeneous solution. Obvious phase changes above the lowest few hundred meters would be observed if the dominant contribution to the homogeneous solution is from modes for which $|D|>H$. In this case the strong, but rapidly damped (in z) driving force could become weaker than the more slowly damped, but initially weaker homogeneous solution at some sufficiently large height, where a sharp phase change may be anticipated. If $|D|<H$ for the dominant modes, phase changes may still occur, but they would probably be relatively inconspicuous, since the driving force would be the strongest at all levels. This reasoning also applies to the former diffusive case for which the homogeneous solution has three vertical modes for each (k,l).

Figs. 6 and 7 of Bonner and Paegle (1970) indicate that, at the surface, the force field produced by the diurnally oscillating temperature above sloping terrain is about twice as strong as the non-terrain contribution over the Great Plains of the United States. If the latter is the gravity wave oscillation under consideration and if $|D|>H$ for the most important modes, this suggests that the homogeneous solution pressure force field has roughly half the amplitude of the terrain slope effect at the surface. In the example, with $D=(978+190i)$ m,

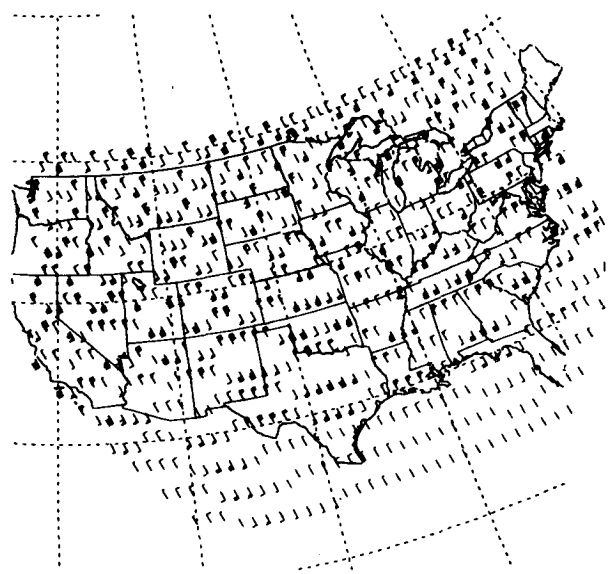

FIG. 4. The amplitude and phase of the diurnal, particular solution surface convergence plotted at 2° latitude, 1° longitude intervals for the frictionless case ($\nu=0$). The amplitudes of the convergence field are plotted like wind speeds, and the phases are plotted as wind directions. A vector directed from the north denotes a maximum convergence at midnight, one from the east denotes a maximum convergence at 0600, etc. Each full barb represents 2×10^{-8} s^{-1}.

the driving force is then most important below 300 m, but the homogeneous solution dominates the terrain effect and the particular solution at higher levels.

The observed force fields described by Thompson *et al.* (1976) over the central United States exhibit pronounced phase changes between 0.5 and 1 km. Consequently, the dominant modes for the homogeneous solution are probably characterized by $|D|>H$. This suggests that the low-level divergence pattern could have a distribution similar to the particular solution.

Finally, the definition of D implies that for the diurnal frequency, and for $\nu=10^{-5}$ s^{-1}, $|D|>H$ for all modes longer than 500 km, regardless of latitude. Thus, the particular solution provides an upper bound surface divergence estimate in all such cases. Moreover, for waves with horizontal wavelength on the order of 1000 km or greater, the total surface divergence is at least 50% of the particular solution surface divergence, and the phase lag is less than about 30°. Therefore, synoptic-scale features in the frictional solution of Eq. (26) provide reasonable upper and lower bound information for the total low-level divergence. However, variabilities on scales $\lesssim$500 km probably give little information for the total solution on the same scales.

4. Experiments

Assuming periodic solutions proportional to $e^{i\omega t}$, Eq. (26) may be rewritten as

$$\{[(i\omega+\nu)^2+f^2]/N^2H^2\}\hat{W}+\nabla^2\hat{W} = g\nabla^2 Z_T(i\omega+\nu)\Upsilon/(H\bar{T})e^{i\omega t}, \quad (35)$$

where $\hat{W}=N^2W$. This equation is solved numerically on a 1° spherical grid extending from 130°W to 70°W and 22°N to 53°N. W is specified zero on the boundaries. The solutions over the United States are insensitive to changes in the boundary condition or placement, for all frictional cases to be displayed.

Fig. 2 displays the input terrain field over the United States. This analysis is based on 1° tabulations of terrain heights, prepared by the U. S. Air Force, archived at the National Center for Atmospheric Research (Jenne and Spangler, 1976). The field is smoothed twice by Shuman's (1957) nine-point filter to eliminate wavelengths of two grid intervals that are not well resolved numerically.

The Laplacian of the terrain height field is displayed in Fig. 3. Positive values represent valley curvatures and negative values represent mountain curvatures. The eastern and western Rocky Mountain regions, as well as the Appalachians, have strongly negative Laplacians. The high plateau of the central Rockies and the Great Plains east of the Rockies have large areas of somewhat weaker positive values.

Fig. 4 displays numerical solutions of $-W/H$ obtained by the solution of (35) for the frictionless case, using the following:

f	$2\omega\sin\phi$	g	9.8 m s^{-2}
ϕ	latitude	$\bar{T}$	300 K
ω	$2\pi/(24$ h$)$	Υ	7 K
N^2	10^{-4} s^{-2}	ν	0.
H	300 m		

$-W/H$ represents the surface convergence of the particular solution, and the depiction is analogous to that used by Wallace (1975). It is assumed that the maximum and minimum surface temperatures occur at 1700 and 0500 CST respectively.

The frictionless solution of Fig. 4 exhibits an abrupt amplitude change about 30°, where the type of the equation changes. The Helmholtz equation (35) changes from boundary value type to wave type poleward of 30° in the frictionless case.

The surface divergence has magnitudes in excess of 10^{-2} s^{-1}, and a rather patchy, small-scale horizontal structure. In this case the particular solution does not give useful information concerning the total solution, as argued in the previous section, and in any case, the present results do not represent interesting upper bounds, but the solution is shown for completeness. There is little or no agreement with Wallace's (1975) observational results (partially reproduced in Fig. 5, with a similar notation as in Fig. 4 referenced to percent thunderstorm occurrences contained in the diurnal period, rather than to convergence).

The unrealistically strong response on short scales is due to the near resonance of numerically resolved waves with the forcing [see Eq. (28)]. Such resonance is only possible in the frictionless case, and explains the pronounced changes that occur as a consequence of even rather small dissipation rates, discussed below.

Fig. 6 displays the particular solutions for low-level divergence with a nonzero damping rate, $\nu=10^{-5}$ s^{-1}. Other parameters are the same as in the previous experiment. This value of ν implies a damping time scale of about 1 day, which may be somewhat long in simulation of actual turbulent boundary layer processes. However, this dissipation rate changes the magnitude and time of maximum divergence greatly. The maximum divergences are now on the order of 3×10^{-4} s^{-1}, and the solution varies smoothly about 30° latitude. There are nocturnal convergence maxima over most of the central United States, while the strongest convergences tend to occur in the afternoon over the Rocky Mountains. In the former region magnitudes do not exceed about 10^{-4} s^{-1}, while peak values in the latter region are about 2×10^{-4} s^{-1}.

Major discrepancies between the convective activity implied in Fig. 6 and observations occur in the vicinity of coastlines, where important seabreezes are excluded in the present approach. There are also strong local nocturnal convergences over portions of the Rocky Mountain Plateau and just west of the Appalachians,

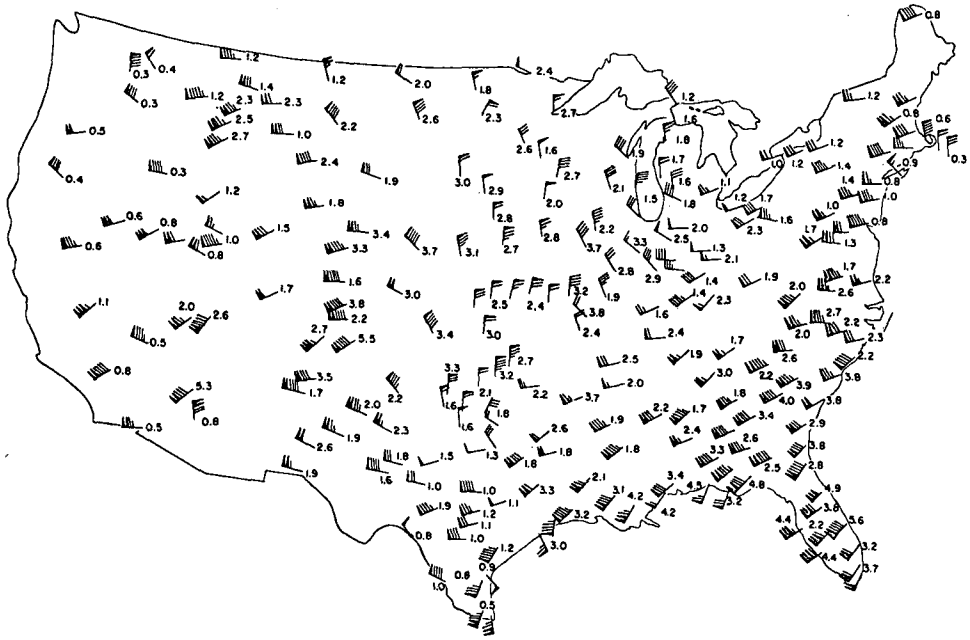

FIG. 5. The diurnal cycle in the observed thunderstorm frequency during the summer season (from Wallace, 1975). The notation is similar to that in Fig. 4, referenced to percent thunderstorm occurrence contained in the diurnal period, rather than to convergence. The numbers plotted beside the stations represent the 24 h average frequencies expressed in terms of percent of the hours with thunderstorm observations.

where afternoon thunderstorm maxima are observed. These smaller scale deviations may be significantly modified by the homogeneous solution or by other terrain resolutions.

Even if the small-scale deviations are actually present in the low-level divergence field their influence on moving air parcels is smoothed as parcels traverse regions of alternating divergence and convergence. Since air parcels moving at speeds on the order of 10 m s^{-1} traverse 400 km over a period of 12 h, it may be appropriate to compare the thunderstorm phasings

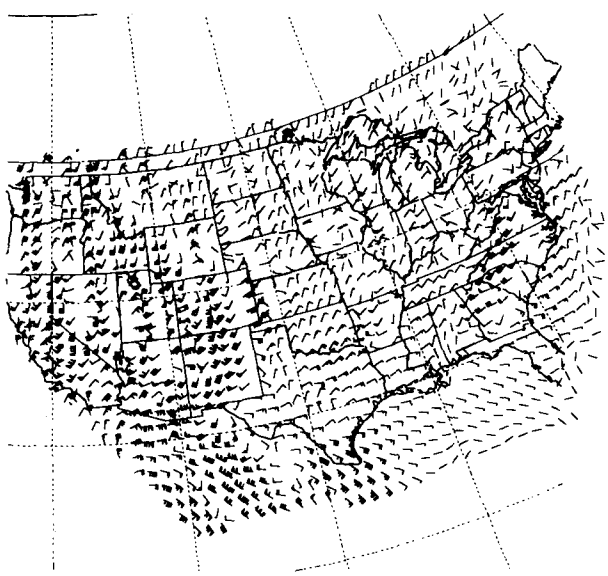

FIG. 6. The amplitude and phase of the diurnal, particular solution surface convergence plotted at 1° latitude, longitude intervals, for the frictional case ($\nu = 10^{-5}$ s^{-1}). Each barb represents 2×10^{-5} s^{-1}.

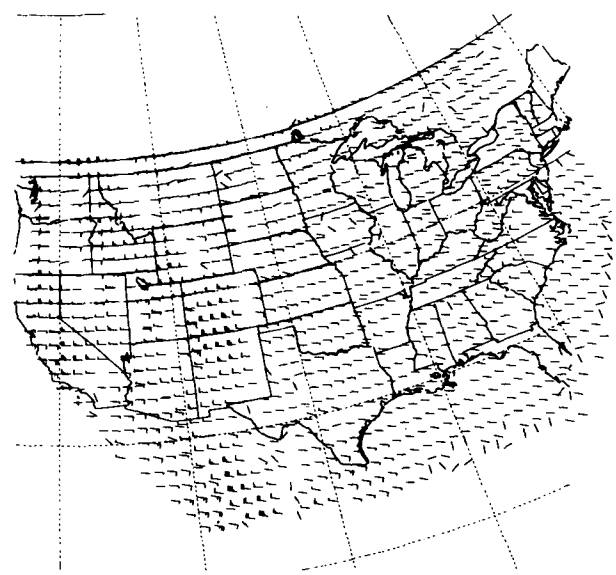

FIG. 7. Amplitude and phase of the diurnal, particular solution surface convergence for the strongly frictional case ($\nu = 10^{-4}$ s^{-1}). The plotting convention is as in Fig. 6.

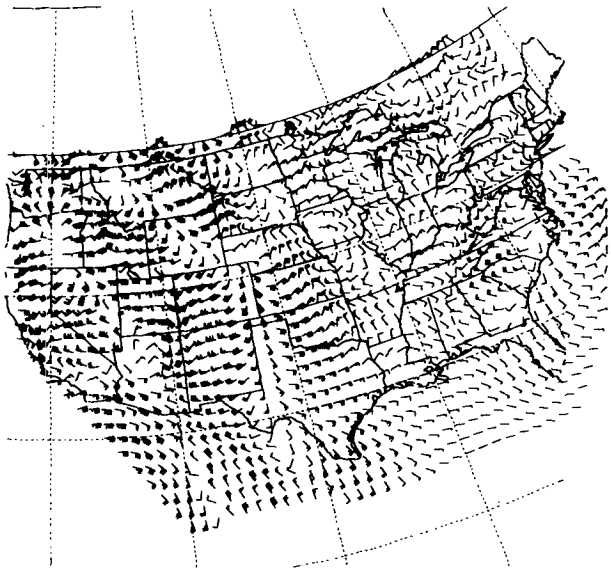

FIG. 8. The amplitude and phase of the diurnal, particular solution surface convergence for the deep thermal forcing case ($\sim e^{-z/800\text{m}}$). The plotting convention is as in Fig. 6.

with corresponding areal averages of the point solutions of Figs. 6–10. The results would be in better agreement with Fig. 5.

Fig. 7 present results for a similar case with $\nu = 10^{-4}$ s^{-1}. Increasing friction by a factor of 10 diminishes the response by about 70% and tends to lock the phases into early morning (central United States) and late afternoon (mountains) convergence maxima. The homogeneous solution may modify the phase by a few hours, but would not increase the amplitude, following the argument of the previous section.

Fig. 8 presents results for $\nu = 10^{-5}$ s^{-1} and $H = 800$ m. This simulates the modification due to stronger low level daytime heating and nocturnal cooling distributed over a greater vertical extent. The strongest surface convergences are diminished to about 50% of those in Fig. 6, and comparisons with Fig. 5 are not improved.

Fig. 9 displays the influence of horizontal variations of static stability N^2 specified as follows:

$N^2 = 10^{-4}$ s^{-2} west of 106°W
$N^2 = 10^{-4}$ s^{-2} $(-\lambda + 105.6)/6$, where λ is in degrees longitude west of Greenwich
$100 \leqslant \lambda \leqslant 105$
$N^2 = 10^{-4}$ s^{-2} east of 100°W.

This experiment is designed to simulate the impact of horizontal stability variations that may be found around a dry line east of the Rockies. There are also certain mathematical analogies to amplified, trapped edge waves on the sloping shore of an ocean (e.g., Reid, 1958). In the present example, it is not possible to have $N^2 = 0$ for numerical reasons, so that the analogy to edge waves on a shoreline is not precise, and the equations are somewhat different from the oceanographic version. Fig. 9 does exhibit some slight changes with respect to Fig. 6, but there are no pronounced amplifications and efficient horizontal ducting is difficult to perceive in the present example.

The final experiment is intended to display the role of the synoptic-scale circulations in modulating the boundary layer convergence response. While it is not possible to include this effect exactly in the linearized equations, an approximation may be appropriate. The nonlinear horizontal equations of motion may be written as

$$\frac{\partial \mathbf{V}}{\partial t} + \Omega \mathbf{K} \times \mathbf{V} = -\nabla[\mathbf{V} \cdot \mathbf{V}/2 + p/\rho] + K\frac{\partial^2 \mathbf{V}}{\partial z^2},$$

where

$$\Omega = f + \mathbf{K} \cdot \nabla \times \mathbf{V}.$$

This type of nonlinear equation was studied by Paegle and Rasch (1973). It was concluded that in the vicinity of circulating synoptic-scale weather features, the diurnal boundary layer response is similar to that of linear models using absolute vorticity Ω in place of f. Therefore, to the extent that those solutions have relevance in the present context, this effect may be locally assessed by varying Ω horizontally to simulate the actual variation of absolute vorticity.

In the present example,

$$\Omega = 2\omega \sin\phi + (2 \times 10^{-5}) \cos[(\lambda - 110)\pi/24] \times \cos[(\phi - 37)\pi/20],$$

where λ (longitude) and ϕ are in degrees and f and ω are in units of s^{-1}. This simulates an anticyclonic center over the southeastern United States, centered roughly

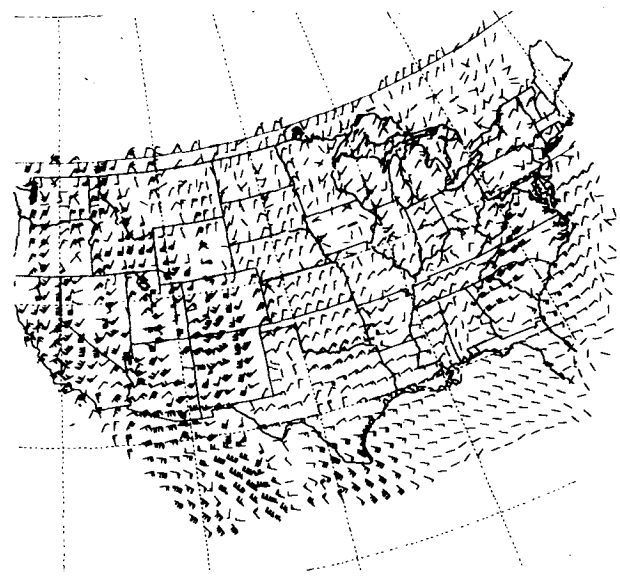

FIG. 9. The amplitude and phase of the diurnal, particular solution surface convergence for the case of spatially varying stratification. The plotting convention is as in Fig. 6.

over Tennessee, and a cyclonic center over northern Arizona. These represent a westward branch of the Bermuda anticyclone and the desert thermal cyclone, respectively. The wavelength of the related flow pattern is about 4400 km, and the horizontal gradients of the absolute vorticity have magnitudes that are similar to the actual meridional gradients of f.

Fig. 10 illustrates the response of the surface convergence field of the particular solution. With the exception of Ω, all parameters are similar to those of Fig. 6. The simulated cyclonic center over the southwestern United States reduces the amplitude of the response there to about one-half of that in Fig. 6. Some of the phases are also noticeably altered. In the southeastern United States the phase of the solution appears to be more sensitive to the anticyclonic circulation than the amplitude.

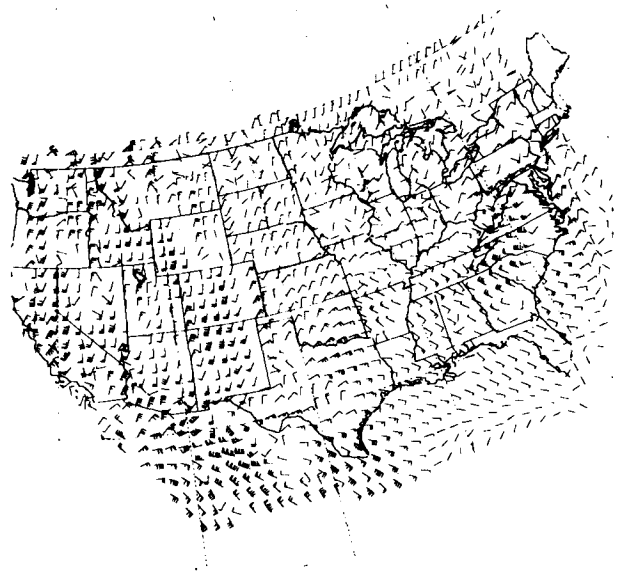

FIG. 10. The amplitude and phase of the diurnal, particular solution surface convergence for the case of spatially variable circulation. The plotting convention is as in Fig. 6.

5. Conclusions

The assumptions of the present analysis may be broadly grouped into three categories: neglected physics, simplified physics, and the actual strength of the mathematical bounds.

Major assumptions in the first category include neglect of time-dependent N^2 and eddy mixing, as well as neglected mid-tropospheric dynamics. Time-dependent stratification could produce trapeze instability, as studied by Orlanski (1973), for a frictionless, nonhydrostatic, flat terrain model that is otherwise similar to the present model. The most unstable modes in that case do not generally occur on the diurnal period, and it is not clear whether the growth rates are sufficiently large to produce a relevant contribution in the present case. However, study of a forced motion, also capable of supporting trapeze instability, could produce a different conclusion.

The neglect of time-dependent eddy mixing may not be critical, according to Paegle and Rasch (1973). They conclude that the major contribution to the diurnal wind oscillations in the planetary boundary layer is due to the terrain effect, and not the diurnal cycle of eddy mixing. However, Yamada and Mellor (1975) simulate significant diurnal wind oscillations in boundary layer models neglecting the terrain effect. The rather sensitive dependence of the present solutions upon friction suggests that time-dependent eddy mixing should be retained in the present model. It would be instructive to study the impact of the fluctuating K theory (first advanced by Blackadar, 1957) on the present time-dependent solutions.

Mahrt and Park (1976) suggest that planetary boundary layer pumping has feedback effects on Rossby waves that can be significant on rather short time scales, and the feedback effects of convection on the boundary layer flow may also be quantitatively important. The present model is incapable of simulating these effects, but they may all be included in more complete numerical approaches.

With respect to simplified physics, it has been assumed that a hydrostatic Boussinesq model, neglecting β effects, is reasonable in the planetary boundary layer. These three assumptions simplify the analysis and the first two would also simplify numerical procedures in a predictive model. They are less important than some of the previously cited omissions, and may be substantiated by scale analysis.

The modeling of viscous effects in a simple drag formulation may not be appropriate because the solutions are quite sensitive to the implied dissipation, and might exhibit similar sensitivity to its formulation. However, the drag formulation is compatible with constant K solutions, provided that $\nu = K/H^2$. Since K is strongly height-dependent in the lower 10–50 m, the present estimates may be reasonable only near the top of this surface layer.

Assuming constant amplitude surface temperature waves and alignment of isentropic surfaces with the terrain may also be inappropriate, and a horizontally uniform exponential decay of the forcing temperature wave with height may not be a reasonable approximation to the actual diurnal temperature wave. Wallace and Patton (1970) find that the vertical decay rates of the diurnal temperature waves observed over most of the United States are nearly exponential through most of the planetary boundary layer, but the damping rate changes by as much as a factor of 2 from the high plateau to the central United States. Given the demonstrated sensitivity of the response to the amplitude and vertical decay of the driving temperature oscillation, these questions deserve further investigation.

The present solutions represent reasonable mathematical upper bounds to the total linear solutions for the given parameter conditions. They suggest that

magnitudes of diurnally oscillating low-level divergence fields have upper bounds of about 10^{-5} to 5×10^{-5} s^{-1} over the nonmountainous central and eastern portions of the United States, and about three times this value over the Rocky Mountains. For horizontal scales of 1000 km or greater, the given solutions, divided by 2, should also represent reasonable lower bounds to the total linear solution. Phase errors should be no greater than 30° on such scales. However, the indicated variables on horizontal scales $\lesssim 500$ km may be greatly modified in the total solution, and it is not known whether the small-scale variabilities in Figs. 6–10 persist in complete solutions.

Low-level divergences with magnitudes $>10^{-5}$ s^{-1} could dominate vertical moisture fluxes out of the planetary boundary layer, even in the presence of high-amplitude, mid-tropospheric disturbances that may produce compensating effects. Thus, the present model is capable of generating low-level divergence fields that could explain the remarkably strong diurnal control of summertime convection over the United States. It is, therefore, reasonable to hypothesize that diurnally oscillating buoyancy forces above even gently sloping terrain are of critical importance in the correct simulation and forecast timing of convective phenomena.

Whether the present estimates provide reasonable bounds to the actual low-level divergence is a separate question, in which the uncertainties due to physical omissions or simplifications arise. The most important evidence for the relevance of the solutions is contained in the data studies of Bonner and Paegle (1970) and Thompson *et al.* (1976). These studies concentrated on the central United States, where the present solutions are in best agreement with the diurnal thunderstorm cycle.

Case-by-case forecasts and further cause-effect studies should relax some of the present physical and mathematical assumptions. It is likely that this can be adequately done only in a fully nonlinear three-dimensional numerical forecast model.

Particular care should be exercised in simulation of the correct evaluation of the low-level temperature field. This may require including a reasonable soil layer, surface layer, and rather detailed vertical resolution of the lowest few hundred meters of the atmosphere. The magnitude of turbulent dissipation may be important, and a reasonable synoptic scale circulation forecast appears to be essential.

Acknowledgments. I wish to acknowledge the generous assistance of Will Spangler and Dennis Shea, both of NCAR, with terrain data and computer graphics, respectively. David W. McLawhorn and anonymous reviewers provided several helpful comments on the manuscript.

REFERENCES

Blackadar, A. K., 1957: Boundary layer wind maxima and their significance for the growth of nocturnal inversions. *Bull. Amer. Meteor. Soc.*, **38**, 283–290.

Bonner, W. D., 1966: Case study of thunderstorm activity in relation to the low-level jet. *Mon. Wea. Rev.*, **94**, 167–178.

——, and J. Paegle, 1970: Diurnal variations in boundary layer winds over the south-central United States in summer. *Mon. Wea. Rev.*, **98**, 735–744.

Garabedian, P. R., 1964: *Partial Differential Equations*. Wiley, 672 pp.

Haltiner, G. J., 1971: *Numerical Weather Prediction*. 317 pp.

Holton, J. R., 1967: The diurnal boundary layer wind oscillation above sloping terrain. *Tellus*, **19**, 199–205.

Jenne, R. L., and W. Spangler, 1976: USAF average elevation data—one degree and 5 minutes. NCAR Manuscript, 8 pp.

Lettau, H., 1967: Small to large-scale features of the boundary layer structure over mountain slopes. *Proc. Symp. Mountain Meteorology*, Dept. Atmos. Sci., Colorado State University, 221 pp.

Lindzen, R. S., and K. K. Tung, 1976: Banded convective activity and ducted gravity waves. *Mon. Wea. Rev.*, **104**, 1602–1617.

Mahrt, L., and S. U. Park, 1976: The influence of boundary layer pumping on synoptic scale flow. *J. Atmos. Sci.*, **33**, 1505–1520.

Ogura, Y., and N. A. Phillips, 1962: Scale analysis for deep and shallow convection in the atmosphere. *J. Atmos. Sci.*, **19**, 173–179.

Orlanski, I., 1973: Trapeze instability as a source of internal gravity waves. Part I. *J. Atmos. Sci.*, **30**, 1007–1016.

Paegle, J., 1969: Studies of diurnally periodic boundary layer winds. Ph.D. thesis, University of California, Los Angeles, 131 pp.

——, and D. W. McLawhorn, 1973: Correlation of nocturnal thunderstorms and boundary layer convergence. *Mon. Wea. Rev.*, **101**, 877–883.

——, and G. E. Rasch, 1973: Three-dimensional characteristics of diurnally varying boundary layer flows. *Mon. Wea. Rev.*, **101**, 746–756.

Pielke, R. A., 1974: A three-dimensional model of the sea breezes. *Mon. Wea. Rev.*, **102**, 115–139.

——, and Y. Mahrer, 1975: Representation of the heated planetary boundary layer in mesoscale models with coarse vertical resolution. *J. Atmos. Sci.*, **32**, 2288–2308.

Reid, R. O., 1958: Effect of Coriolis force on edge waves (I) Investigation of the normal modes. *J. Mar. Res.*, **16**, 109–143.

Shuman, F. G., 1957: Numerical methods in weather prediction. II. Smoothing and filtering. *Mon. Wea. Rev.*, **85**, 357–361.

Thompson, O. E., P. A. Arking and W. D. Bonner, 1976: Diurnal variations of the summertime wind and force field at three midwestern locations. *Mon. Wea. Rev.*, **104**, 1012–1022.

Wallace, J. M., 1975: Diurnal variations in precipitation and thunderstorm frequency over the conterminous United States. *Mon. Wea. Rev.*, **103**, 406–419.

——, and D. B. Patton, 1970: Diurnal temperature variations: Surface to 25 kilometers. *Mon. Wea. Rev.*, **98**, 548–552.

Welch, R. M., J. Paegle and W. G. Zdunkowski, 1978: Two-dimensional numerical simulation of the effect of air pollution upon the urban-rural complex. *Tellus* (in press).

Yamada, T., and G. Mellor, 1975: A simulation of the Wangara atmospheric boundary layer data. *J. Atmos. Sci.*, **32**, 2309–2329.